# Experimental Demonstration of Quasi-resonant Absorption in Silicon Thin Films for Enhanced Solar Light Trapping

Ardavan Oskooi,* Menaka De Zoysa, Kenji Ishizaki, and Susumu Noda

Department of Electronic Science & Engineering, Kyoto University, Kyoto 615-8510, Japan

ABSTRACT: We experimentally demonstrate that the addition of partial lattice disorder to a thin-film microcrystalline silicon photonic crystal results in the controlled spectral broadening of its absorption peaks to form quasi resonances: increasing light trapping over a wide bandwidth while also reducing sensitivity to the angle of incident radiation. Accurate finite-difference time-domain simulations are used to design the active-layer photonic crystal so as to maximize the number of its absorption resonances over the broadband interval where microcrystalline silicon is weakly absorbing before lattice disorder augmented with fabrication-induced imperfections is applied to further boost performance. Such a design strategy may find practical use for increasing the efficiency of thin-film silicon photovoltaics.

**KEYWORDS:** solar light trapping, nanophotonics, photovoltaics, photonic crystals
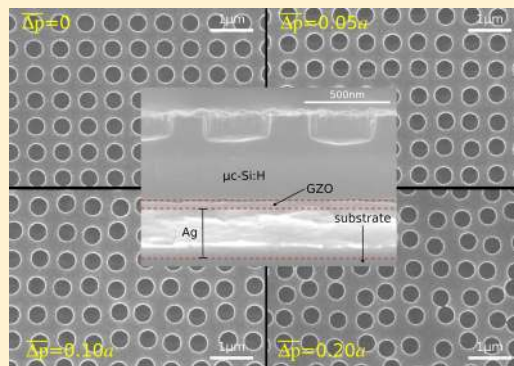
A key component of a thin-film silicon photovoltaic (PV) cell is a light-trapping structure that provides enhanced absorption of solar radiation over a broad range of frequencies and incident angles.[1] While there have been numerous proposals of nanostructured designs exploiting resonant wave effects of photons for this purpose including surface plasmons,[2] nanowires,[3] photonic crystals,[4,5] nanostructured back reflectors,[6−8] and surface gratings,[9,10] most have been limited by inherent delicate-interference effects to a restricted set of operating conditions involving narrow bandwidths, select polarizations, or a small angular cone. We recently introduced a new mechanism for photon absorption in thin films based on the notion of *quasi* resonances, which combine the large absorption of impedance-matched resonances with the broadband and robust characteristics of disordered systems.[11] Furthermore, we showed that such an approach can significantly exceed the Lambertian light-trapping limit—the maximum possible for optically thick wafer cells employing random scattering of light rays—over a wide range of conditions.[12] A related work explored the design of a surface diffraction grating based on a quasi-random structure by carefully tuning its Fourier spectra to scatter incident light into the guided modes of a thin film.[13] This differs from our approach, which is based on the controlled spectral broadening of absorption peaks with disorder starting from a perfect lattice that enables us to tailor with better precision an absorption profile that is more uniform with fewer gaps and thus has better light-trapping performance. In this letter, we experimentally demonstrate using conventional semiconductor nanofabrication processes potentially applicable to large-scale thin-film PV manufacturing how quasi resonances can be used to increase the light-trapping performance of a microcrystalline silicon (μc-Si:H) thin film by applying partial lattice disorder to an active-layer photonic crystal (PC) in order to precisely control the spectral broadening of its resonant-absorption peaks. We employ computational design based on accurate finite-difference time-domain (FDTD) simulations[14,15] to structure a thin-film PC slab to contain as many absorption resonances as possible over a broad bandwidth where μc-Si:H is weakly absorbing and also, given the consistency of the numerical and experimental results, use such simulations to investigate parasitic absorption in the rest of the device, which is precluded by an experimental approach alone. Finally, we show how the presence of unintentional fabrication-induced imperfections can be harnessed together with intentional lattice disorder to further enhance light trapping over a broad bandwidth and angular range.

A substrate-type thin-film μc-Si:H PV cell with light-trapping capability is typically fabricated by depositing the active layer on a textured back reflector such that the pattern is then transferred throughout the entire device.[8,16] This specific design however has two principal disadvantages: first, patterning of the metallic layer may enhance unwanted plasmonic losses[17] and, second, the μc-Si:H layer must be grown on a nonuniform surface, which due to the onset of more grain boundaries and defects during film growth, acts as recombination centers, degrading its charge-transport properties.[16] As a result, in this work we take a different approach and form the light-trapping structure directly within only the active layer itself. Our device, a precursor to a fully functional PV cell, is fabricated on top of a base substrate using conventional thin-film deposition tools as follows. First, a back reflector consisting of a 270 nm silver (Ag) film is placed on the substrate via
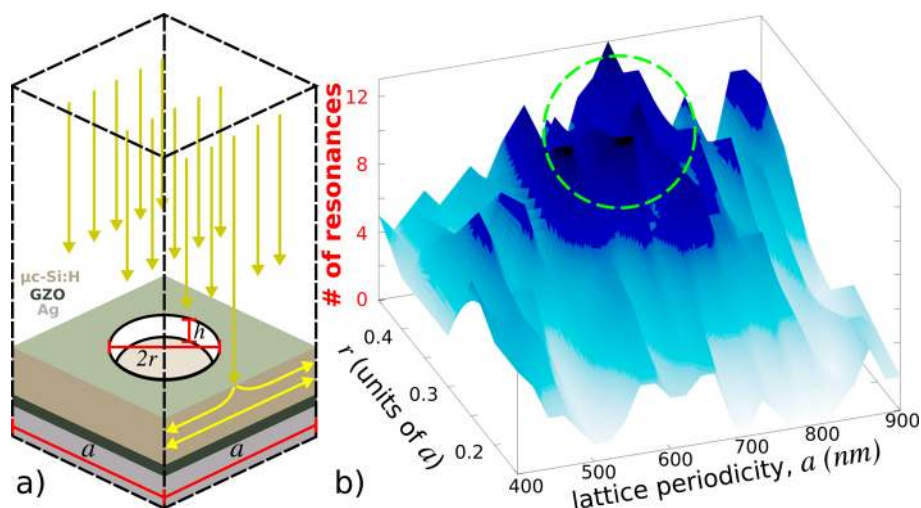
Figure 1. The μc-Si:H PC active layer is computationally designed to maximize the number of its absorption resonances, which is correlated with its light-trapping efficiency.[12] (a) Schematic of the unit cell for the thin-film PC device used in the FDTD simulations to compute the absorptivity spectra at normal incidence. The PC consists of a square lattice of holes in the μc-Si:H layer with periodicity a, hole radius r, and height h. (b) 3D contour plot of the number of resonances—obtained from the simulated absorptivity spectra by using constant peak-identification threshold criteria of 80% absorptivity with no other constraints—plotted over the 2D parameter space of PC lattice periodicity a and hole radius r (hole height h is fixed at 180 nm). The region containing the largest values is circled.
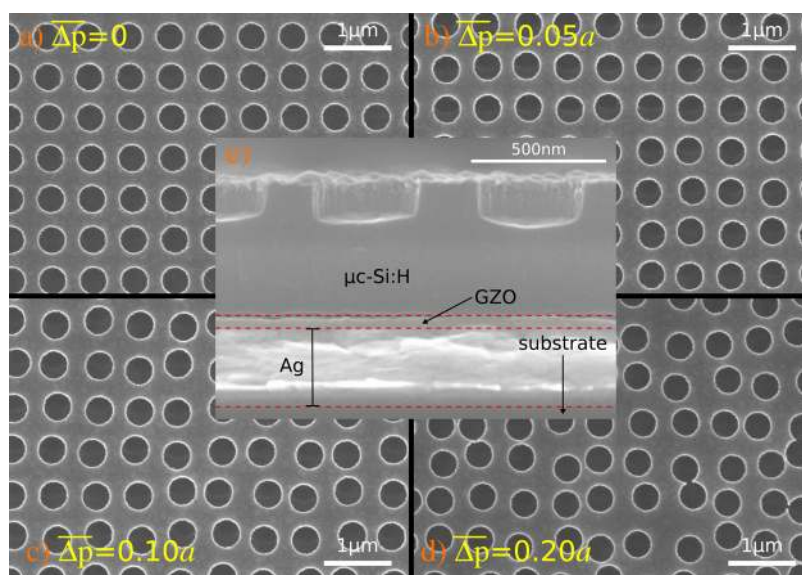

Figure 2. Scanning electron microscopy (SEM) images of the thin-film light-trapping device showing four partially disordered PC lattices in (a)−(d): the hole positions of the perfect lattice have been perturbed by an amount Δp chosen randomly from a uniform distribution of values between 0 and $\overline{\Delta p}$ for both orthogonal in-plane directions. The disorder quantity is given in units of the square-lattice parameter, a. (e) SEM image of the device cross section showing all three individual layers: silver (Ag), gallium-doped zinc oxide (GZO), and μc-Si:H. Note the uneven profile of the etched holes in the μc-Si:H, which will cause a slight degree of intrinsic broadening in the film's absorption peaks.

electron-beam evaporation. Next, a thin, 40 nm layer of gallium-doped zinc oxide (GZO) with carrier density and mobility of 5×10^{19} cm^{-3} and 18 cm^2/(V s) is sputtered on top followed by growth of the main active layer: 510 nm of intrinsic μc-Si:H via plasma-enhanced chemical vapor deposition (PECVD) with hydrogen (H$_2$) and silane (SiH$_4$) feed-in gases. The crystallinity fraction of the μc-Si:H film is found using Raman spectroscopy to be 59% by fitting it to a combination of the known spectra of amorphous and crystalline silicon.[18] Then, electron-beam lithography is used to define the two-dimensional PC pattern over an area of 2107 × 2107 periods of the square lattice (approximately 1.5 mm^2) in the spun-on positive resist, which is followed by inductively

coupled plasma (ICP) reactive-ion etching (RIE) to create arrays of cylindrically shaped holes on the top surface. Lastly, the resist residue is removed by soaking the samples in trichloroethylene followed by O$_2$ plasma ashing. Note that while this device is sufficient for investigating the optical-absorption characteristics of the active μc-Si:H layer, the focus of this work, it can be readily extended to a complete PV cell through an additional three processing steps: growing a p-doped μc-Si:H layer on top of a hole-etched intrinsic layer that sits above an n-doped layer to form an n−i−p junction, sputtering another layer of transparent conductive oxide (e.g., ITO) with a thickness of roughly 70 nm on top of this μc-Si:H layer, and finally depositing a finger-grid of silver electrodes on
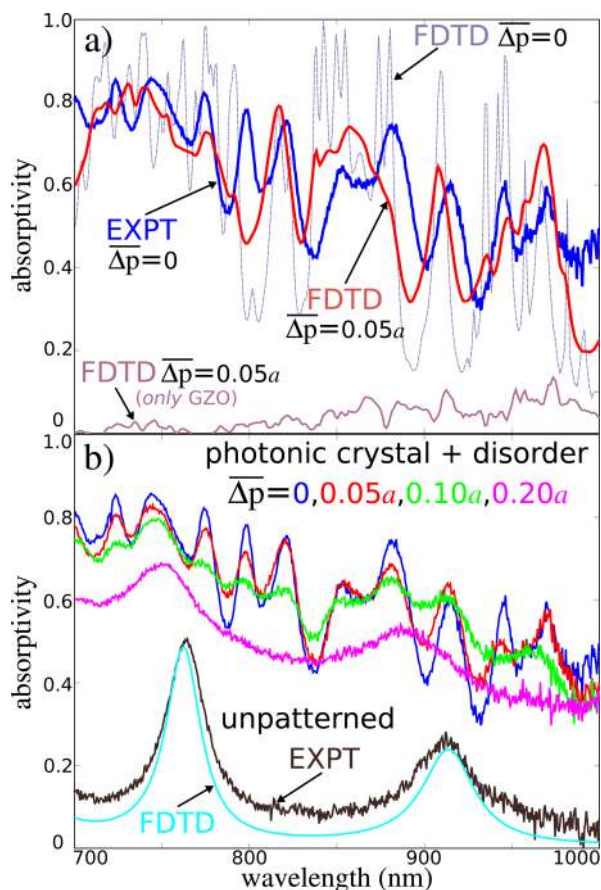
Figure 3. (a) Comparison of the absorptivity spectra of the μc-Si:H thin-film PC device for s-polarized light at an angle of incidence of 10°. The experimental data for the device with no disorder ($\overline{\Delta p}$ = 0, in blue) measured using an integrating sphere show good agreement with the FDTD calculation with small disorder ($\overline{\Delta p}$ = 0.05a, in red), indicating the presence of intrinsic imperfections. The absorption within just the GZO layer in gray as computed by simulations is only a small fraction of the overall total. (b) Experimental absorptivity data under the same measurement conditions demonstrating gradual broadening of the absorption peaks with increasing disorder in the PC device. The unpatterned μc-Si:H film (in black) is shown for reference with the corresponding FDTD calculation (in cyan); the minor discrepancy arises from the incomplete collection of light within the integrating sphere, which appears as a constant background absorption.

the front surface. The electron-beam lithography and dry plasma etching used here to create a prototype design can be easily replaced by standard photolithography followed by a wet etch, which is more practical for large-area fabrication.[8] Etching holes into the μc-Si:H film will likely tend to increase charge recombination effects and thus lower the open-circuit voltage;[19] however, if the holes can be made both sufficiently small and smooth[20] while still retaining features of the Bloch modes and be passivated by the transparent conductive oxide film grown on top similar to other approaches,[21] the impact of such film-quality degradation may be mitigated while still providing many more degrees of design freedom in the choice of lattice for light trapping.

The thin-film PC structure that maximizes the light-trapping efficiency, a figure of merit we defined previously in ref 11, can be obtained from a two-part design strategy:[12] (1) maximize the number of *resonant-absorption modes* and (2) apply a partial

amount of disorder to boost broadband light trapping and robustness. While we have already shown that there exists a close correlation between the number of absorption resonances and the light-trapping efficiency,[12] it is worthwhile to reiterate that the design process is facilitated by the former due to both its direct connection to quasi resonances and better suitability as an objective function for topology optimization where a gradient-free search of a large parameter space is necessary. This is the case even though the latter, which is proportional to the short-circuit current, is a more explicit measure of PV cell performance. For the first step, we use the open-source FDTD software tool Meep[14] to exhaustively explore the PC design space consisting of just two parameters in its unit cell as shown in the schematic of Figure 1a: the lattice periodicity and hole radius (the hole height is fixed at 180 nm, a somewhat arbitrary value that nonetheless gives rise to meaningful results). In order to ensure that the absorptivity spectra of our computational design agrees well with its experimental realization, we need to accurately incorporate the full complex-refractive index profile of μc-Si:H over a broad bandwidth into the FDTD simulations. Here we focus on the wavelength interval spanning 700 to 1000 nm, where the absorption coefficient of μc-Si:H is small (less than approximately 1000 cm^{-1} and decreasing[18]) and thus the need for a light-trapping design is most relevant. As it turns out, in this specific regime the complex-refractive index profile of μc-Si:H is very similar to that of crystalline silicon (c-Si),[18,22] allowing us to make use of the extensively compiled data of the latter.[23] We therefore perform a nonlinear fit of the c-Si experimental data to a slightly modified Drude−Lorentzian polarizability term used in the FDTD simulations[12] and obtain a close match in both the real part of the refractive index and the absorption coefficient. For even greater accuracy, we also incorporate into the simulations the material losses of GZO used in our actual device by first measuring its absorptivity in a separate experiment and then from this computing its absorption coefficient using a transfer-matrix approach.[24] We will demonstrate later on that though GZO's absorption coefficient may be large relative to that of μc-Si:H (particularly at long wavelengths), nevertheless its absorption as a fraction of the total in the overall device is insignificant given that it is so much thinner and placed behind the μc-Si:H layer. Figure 1b shows a contour plot of the number of absorption resonances—obtained from the simulated absorptivity spectra at normal incidence where the peak-identification threshold criteria are taken to be a constant 80% absorptivity at all wavelengths with no constraints on the peaks' width or spacing relative to other peaks—as a function of the lattice periodicity and radius. The dotted green circle denotes the region where the number of peaks is largest and from which we select exemplary PC parameters for fabrication: a = 650 nm and r = 208 nm.

The fabricated PC device along with three of its partially disordered variants where the position of the holes in the perfect lattice has been perturbed by an amount Δp chosen randomly from a uniform distribution of values between 0 and $\overline{\Delta p}$ for both orthogonal in-plane directions ($\overline{\Delta p}$ = 0.05a, 0.10a, 0.20a) is shown in Figure 2a−d. Some slight nonuniformity is evident in the hole shapes, which will naturally tend to broaden the sharp absorption peaks found in the otherwise perfect case, as will be apparent soon. A cross section of the entire device is shown in Figure 2e, where the three individual layers can be seen as well as the profile of the etched holes, with its somewhat uneven morphology, which also contributes to the
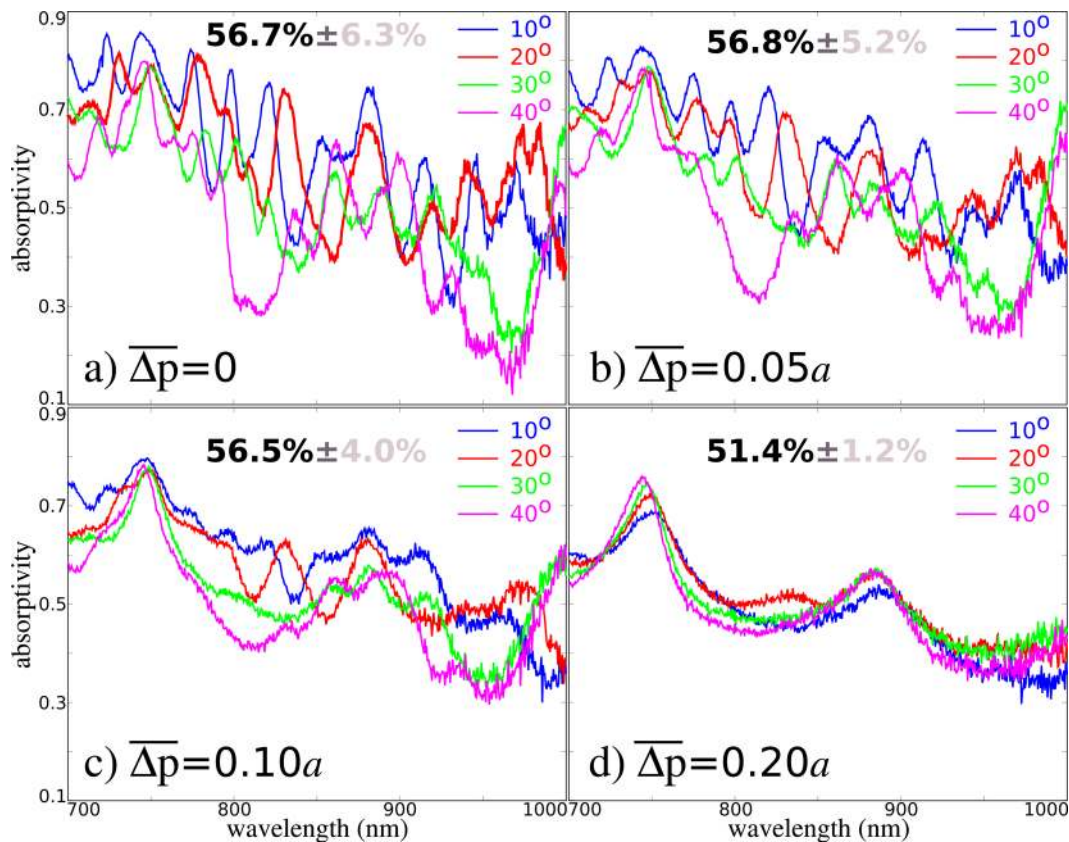
Figure 4. Experimental absorptivity data of four partially disordered PC devices ($\overline{\Delta p}$ = 0, 0.05a, 0.10a, 0.20a) in (a)−(d) for s-polarized light at four angles of incidence, 10°, 20°, 30°, and 40°, where the average light-trapping efficiency (as calculated over these four angles) and corresponding standard deviation are indicated. The device with nearly maximum light-trapping efficiency in (c) with $\overline{\Delta p}$ = 0.10a is nearly a 10% efficiency improvement above and nearly twice as robust as the ideal nonperturbed design.

intrinsic imperfections affecting device performance. The presence of surface roughness on the μc-Si:H film with feature sizes of less than 20 nm does not significantly affect the absorption properties of the device, unlike the irregularities associated with the holes, which we confirmed separately with simulations; this is to be expected since the latter form the primary scattering objects of the lattice and thus more strongly influence the delicate-interference effects underlying the coherent nature of the guided resonant modes.

Next we measure the absorptivity spectra via 1-reflectivity of the unperturbed ($\overline{\Delta p}$ = 0) sample in an integrating sphere connected to a spectrometer and multichannel Si detector using a tungsten-halogen lamp source with a 610 nm low-pass filter for s-polarized light at an angle of incidence of 10°. Here polarized light enables us to more clearly observe the resonant features of the absorption, although in practical solar applications both polarizations must be taken into consideration. The results, shown in Figure 3a (in blue), display traces of numerous absorption resonances but all have noticeably undergone a minor degree of broadening due to the nonuniformities inherent in the holes' morphology as discussed previously. This becomes evident when these experimental results are compared with those from two FDTD simulations (computed using identical incident-light conditions to the experimental measurements): one for $\overline{\Delta p}$ = 0 and the other for $\overline{\Delta p}$ = 0.05a, where good agreement is apparent between the fabricated sample with $\overline{\Delta p}$ = 0 and the simulated one with $\overline{\Delta p}$ = 0.05a (here three separate simulations are made using a 10 × 10 supercell, and the absorptivity spectra are averaged due to

the random nature of the design). This therefore suggests that from the perspective of light trapping the amount of intrinsic imperfections present within the fabricated sample is approximately equivalent to a lattice disorder of $\overline{\Delta p}$ = 0.05a, which is sufficiently minor so as to still confer an overall benefit to the device performance. Also shown in Figure 3a is the absorptivity spectra of just the GZO layer for the $\overline{\Delta p}$ = 0.05a device (computed in FDTD again with three separate simulations by subtracting the absorptivity of the device with GZO absorption from one without, which though not exact is still mostly accurate), demonstrating the relatively small absorption in this very thin, 40 nm layer that tends to increase somewhat with wavelength as the absorption coefficient of μc-Si:H becomes smaller. The discrepancies between the experimental and simulated results, particularly at large wavelengths near 1000 nm, can be attributed to two primary reasons: (1) the disparity between the complex-refractive index of μc-Si:H of the fabricated device and the c-Si used in the simulations,[18,22] especially when the absorption coefficient is small, as it is at large wavelengths, which produces pronounced differences in the resulting absorptivity spectra due to lattice effects, and (2) the reduced signal-to-noise ratio of the measured data at large wavelengths due to the diminishing intensity from the tungsten-halogen input source. Figure 3b shows the measured absorptivity spectra of the four PC samples and demonstrates gradual broadening of the resonant-absorption peaks with increasing disorder and thus the onset of quasi resonances consistent with our prior observations.[11] Note however that the absorptivity spectrum for the $\overline{\Delta p}$ =

0.20*a* device shows no traces of the resonant modes, indicating that the amount of partial lattice disorder necessary to broaden the absorption peaks to the maximal extent without destroying them altogether—the key principle for creating quasi resonances with optimal light-trapping characteristics[11]—in the actual fabricated samples as a result of the intrinsic imperfections is markedly less than that of the ideal designs typically used in the simulations. The absorptivity spectra of the same device with an unpatterned μc-Si:H layer is also shown for reference with its broad Fabry−Pérot resonances, where in the absence of a light-trapping structure the absorptivity at each wavelength over the entire interval is considerably less than that of its partially disordered PC counterparts. The corresponding data from an FDTD simulation are also shown for comparison to highlight both the presence and quantity of constant background absorption in the experiments due to the incomplete collection of light within the integrating sphere, which occurs since some of the specularly reflected light from the device unavoidably escapes from the entrance port.

We continue to experimentally measure the angular dependence of the absorptivity spectra of the perfect and three partially disordered thin-film PC devices in Figure 4 at four angles of incidence, 10°, 20°, 30°, and 40°, again for incident s-polarized light. The performance of each device is quantified using its light-trapping efficiency averaged over the four angles as well as its standard deviation to gauge robustness. Though the efficiency is calculated using the broadband absorption of the entire device, which includes that of the GZO layer, the results are still relevant for assessing the performance of a potential PV cell primarily because the GZO absorption is relatively small, as was demonstrated earlier. Figure 4a shows just how sensitively the position of the resonant-absorption peaks of the unperturbed PC structure depends on the incident conditions and the degree to which this can be made less and less so with the gradual addition of disorder, just as we had previously observed with simulations.[11] The light-trapping efficiency increases with partial lattice disorder (attaining a maximum of 56.8% at $\overline{\Delta p}$ = 0.05*a* in Figure 4b) before decreasing considerably to 51.4% at $\overline{\Delta p}$ = 0.20*a* while the robustness continually improves (the standard deviation of the efficiency decreases) with disorder, again generally consistent with our earlier findings.[11] The dual integration of lattice disorder and fabrication imperfections is perhaps best represented by the nearly optimal partially disordered PC device with $\overline{\Delta p}$ = 0.10*a* (in Figure 4c), which is nearly 10% more efficient and more than twice as robust as the ideal design (47.9 ± 8.2%) as computed by simulations.

In summary, we have experimentally shown how quasi resonances can be incorporated into a thin-film silicon device as a PC with a controlled amount of partial lattice disorder augmented with unintentional fabrication-induced imperfections to boost light trapping over a broad bandwidth and angular range. The design process was enabled by accurate FDTD simulations to both structure the active-layer PC and to investigate parasitic absorption in the rest of the device. A further extension of this design strategy to a complete thin-film μc-Si:H PV cell possibly based on the guidelines we have outlined is the next step for investigating the role of quasi resonances in increasing overall efficiency.

■ **AUTHOR INFORMATION**

Corresponding Author
*E-mail: oskooi@qoe.kuee.kyoto-u.ac.jp.

■ **REFERENCES**
(1) Poortmans, J.; Arkhipov, V. *Thin Film Solar Cells: Fabrication, Characterization and Applications*; John Wiley & Sons, Ltd, 2006.
(2) Atwater, H.; Polman, A. Plasmonics for improved photovoltaic devices. *Nat. Mater.* **2010**, *9*, 205−213.
(3) Garnett, E.; Yang, P. Light trapping in silicon nanowire solar cells. *Nano Lett.* **2010**, *10*, 1082−1087.
(4) Zhou, D.; Biswas, R. Photonic crystal enhanced light-trapping in thin film solar cells. *J. Appl. Phys.* **2008**, *103*, no. 093102.
(5) Mallick, S.; Agrawal, M.; Peumans, P. Optimal light trapping in ultra-thin photonic crystal crystalline silicon solar cells. *Opt. Express* **2010**, *18*, 5691−5706.
(6) Bermel, P.; Luo, C.; Zeng, L.; Kimerling, L.; Joannopoulos, J. Improving thin-film crystalline silicon solar cell efficiencies with photonic crystals. *Opt. Express* **2007**, *15*, 16986−17000.
(7) Hsu, C.-M.; Battaglia, C.; Pahud, C.; Ruan, Z.; Haug, F.-J.; Fan, S.; Ballif, C.; Cui, Y. High-efficiency amorphous silicon solar cell on a periodic nanocone back reflector. *Adv. Ene. Mater.* **2012**, *2*, 628−633.
(8) Sai, H.; Saito, K.; Kondo, M. Enhanced photocurrent and conversion efficiency in thin-film microcrystalline silicon solar cells using periodically textured back reflectors with hexagonal dimple arrays. *Appl. Phys. Lett.* **2012**, no. 173901.
(9) Han, S.; Chen, G. Toward the lambertian limit of light trapping in thin nanostructured silicon solar cells. *Nano Lett* **2010**, *10*, 4692−4696.
(10) Sheng, X.; Liu, J.; Kozinsky, I.; Agrawal, A.; Michel, J.; Kimerling, L. Design and non-lithographic fabrication of light trapping structures for thin film silicon solar cells. *Adv. Mater.* **2011**, *23*, 843−847.
(11) Oskooi, A.; Favuzzi, P.; Tanaka, Y.; Shigeta, H.; Kawakami, Y.; Noda, S. Partially-disordered photonic-crystal thin films for enhanced and robust photovoltaics. *Appl. Phys. Lett.* **2012**, *100*, no. 181110.
(12) Oskooi, A.; Tanaka, Y.; Noda, S. Tandem photonic-crystal thin films surpassing lambertian light-trapping limit over broad bandwidth and angular range. *Appl. Phys. Lett.* **2014**, *104*, no. 091121.
(13) Martins, E.; Li, J.; Liu, Y.; Depauw, V.; Chen, Z.; Zhou, J.; Krauss, T. Deterministic quasi-random nanostructures for photon control. *Nat. Commun.* **2013**, *4*, 2665.
(14) Oskooi, A. F.; Roundy, D.; Ibanescu, M.; Bermel, P.; Joannopoulos, J. D.; Johnson, S. G. MEEP: A flexible free-software package for electromagnetic simulations by the FDTD method. *Comput. Phys. Commun.* **2010**, *181*, 687−702.
(15) Taflove, A.; Oskooi, A.; Johnson, S., Eds. *Advances in FDTD Computational Electrodynamics: Photonics and Nanotechnology*; Artech House, 2013.
(16) Python, M.; Madani, O.; Domine, D.; Meillaud, F.; Vallat-Sauvain, E.; Ballif, C. Influence of the substrate geometrical parameters on microcrystalline silicon growth for thin-film solar cells. *Sol. Ener. Mat. Sol. Cells* **2009**, *93*, 1714−1720.
(17) Palanchoke, U.; Jovanov, V.; Kurz, H.; Obermeyer, P.; Stiebig, H.; Knipp, D. Plasmonic effects in amorphous silicon thin film solar cells with metal back contacts. *Opt. Express* **2012**, *20*, 6340−6347.
(18) Vallat-Sauvain, E.; Shah, A.; Bailat, J. *Advances in Microcrystalline Silicon Solar Cell Technologies*; John Wiley & Sons, Ltd., 2006; Chapter 4.

(19) Soderstrom, T.; Haug, F.-J.; Terrazzoni-Daudrix, V., Ballif, C. Optimization of amorphous silicon thin film solar cells for flexible photovoltaics. *J. Appl. Phys.* **2008**, *103*, no. 114509.

(20) Sai, H.; Fujiwara, H.; Kondo, M.; Kanamori, Y. Enhancement of light trapping in thin-film hydrogenated microcrystalline Si solar cells using back reflectors with self-ordered dimple pattern," *Appl. Phys. Lett.* **2008**, no. 143501.

(21) Lauinger, T.; Schmidt, J.; Aberle, A.; Hezel, R. Record low surface recombination velocities on 1σcm psilicon using remote plasma silicon nitride passivation. *Appl. Phys. Lett.* **1996**, *68*, 1232−1234.

(22) Vetterl, O.; Finger, F.; Carius, R.; Hapke, P.; Houben, L.; Kluth, O.; Lambertz, A.; Muck, A.; Rech, B.; Wagner, H. Intrinsic microcrystalline silicon: a new material for photovoltaics. *Sol. Ener. Mat. Sol. Cells* **2000**, *62*, 97−108.

(23) Green, M. Self-consistent optical parameters of intrinsic silicon at 300 k including temperature coefficients. *Sol. Energy Mater. Sol. Cells* **2008**, *92*, 1305−1310.

(24) Yeh, P. *Optical Waves in Layered Media*; Wiley: New York, 1988.